Evaluation of three spatial discretization schemes with the Galewsky et al. test

Seoleun Shin* Matthias Sommer** Sebastian Reich* Peter Névir**

February 22, 2010

Abstract

We evaluate the Hamiltonian Particle Methods (HPM) and the Nambu discretization applied to shallow-water equations on the sphere using the test suggested by Galewsky et al. (2004). Both simulations show excellent conservation of energy and are stable in long-term simulation. We repeat the test also using the ICOSWP scheme to compare with the two conservative spatial discretization schemes. The HPM simulation captures the main features of the reference solution, but wave 5 pattern is dominant in the simulations applied on the ICON grid for this highly idealized test. As the spatial resolution increases, the wave 5 pattern weakens and features of reference solution emerge on the ICON grid. Nevertheless, agreement in statistics between the three schemes indicates their qualitatively similar behaviours in the long-term integration.

1 Introduction

For long-term simulations of atmospheric flows, it is essential to develop numerical schemes that retain conservation properties such as mass, energy, circulation, and locally potential vorticity or globally potential enstrophy. Potential vorticity (PV) is one of the quantities of main interest in atmospheric flows. It is advected materially along the path of fluid particles. Particle methods are a fully Lagrangian formulation and maintain PV as well as other conservation properties in a long-term simulation. The discretized Hamiltonian approach used in particle methods leads to methods preserving the symplecticity of fluid flows. This makes them an attractive alternative to Eulerian atmospheric models. However, the generation of high-frequency waves is a challenge in their applications. The problem is dealt with by regularization in such way that the conservation properties are not affected. Consequently, artificial diffusion can be avoided and time-reversibility survives. The Hamiltonian particle-mesh (HPM) method has been proposed by Frank et al. (2002) for shallow-water equations in planar geometry and extended to the shallow-water equations on the sphere (Frank &

*Universität Potsdam, Institut für Mathematik, Am Neuen Palais 10, D-14469 Potsdam, Germany

**Freie Universität Berlin, Institut für Meteorologie, Carl-Heinrich-Becker-Weg 6–10, D-12165 Berlin, Germany

Reich 2004). Also non-hydrostatic HPM simulations have been presented recently in Shin & Reich (2009).

Névir & Blender (1993) extended the Nambu mechanics to incompressible hydrodynamics to generalize the non-canonical Hamiltonian formulation. Salmon (2005) and Salmon (2007) combined this idea with the general strategy of using antisymmetry properties to construct numerical schemes that conserve mass, circulation, energy, and potential vorticity. His idea is adopted by Sommer & Névir (2009) for the shallow-equations on a staggered geodesic grid used for the ICOsahedral Non-hydrostatic (ICON) model. Besides conservation of energy and enstrophy, they show numerically that such schemes are stable and reproduce spectral properties of underlying partial differential equations.

Here we further evaluate the HPM and the Nambu schemes by using a test proposed by Galewsky et al. (2004). They use simple analytical functions for the initial perturbation to represent barotropically unstable zonal flow, from which complex dynamics is generated. More details and the given analytic function can be found in Galewsky et al. (2004). First, we examine the ability of the HPM and the Nambu schemes to maintain a steady zonal jet in the absence of the perturbation. Then vorticity fields are compared to examine to which extent features of reference solution are captured for the generation of barotropic instability. Also we run long-term simulations and analyze spectral distribution and time series to investigate the long-term behaviour of each discretization for this test.

In the next section we describe the test briefly and introduce main properties of the HPM and the Nambu discretization. In section 3 results from simulations are presented and discussed. Lastly we evaluate our schemes and suggest outlook for further studies.

2 Description of the test case and numerical schemes

2.1 Test case

The mentioned test case is designed for the evaluation of the behaviour of numerical discretization schemes for the shallow-water equations 2.1 and 2.2. These equations describe the flow of a shallow fluid on a rotating sphere and can be written as

$$\partial_t \mathbf{v} = -\mathbf{v} \cdot \nabla \mathbf{v} - f\mathbf{k} \times \mathbf{v} - g\nabla h \tag{2.1}$$

$$\partial_t h = -\nabla \cdot (h\mathbf{v}). \tag{2.2}$$

The variables are defined as:

$\mathbf{v}$	Horizontal velocity vector
h	Height of the fluid
f	Coriolis parameter
$\mathbf{k}$	Vertical unit vector

Here we include no diffusion terms. More details of the HPM and the Nambu representation of the shallow-water model can be found in Frank & Reich (2004) and Sommer & Névir (2009). In the following subsections we introduce properties of each scheme briefly. The initial condition given in this test is depicted in Figure 1. The basic zonal wind of 80 ms^{-1} represents a mid-latitude tropospheric jet, and the height is geostrophically balanced with the wind field. A small unbalanced perturbation to the height field is added at the initial

time, which generates barotropic instability. This perturbation is specified analytically so that the initial condition given by Galewsky et al. (2004) is easily reproduced.

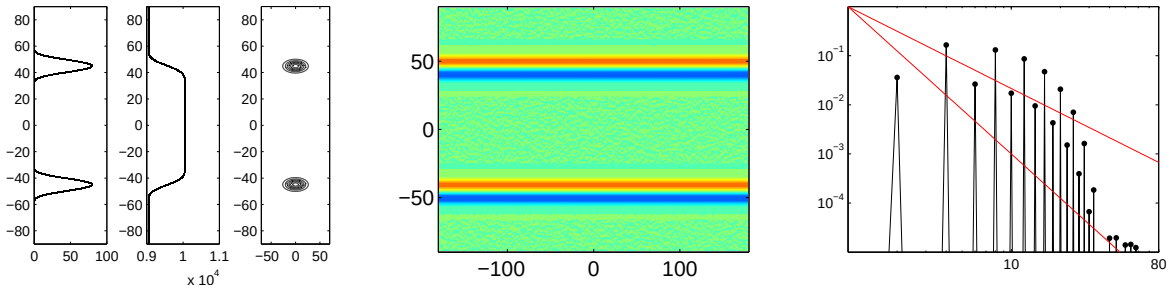

Figure 1: Wind field representing jet flow, geostrophically balanced height field, and height perturbation (left); vorticity field (middle); spectrum at $t = 0$ (right).

2.2 The ICON scheme

The grid structure of ICON shallow-water model (ICOSWP) (Bonaventura & Ringler 2005) is illustrated in Fig. 2. The Weber transformation $\mathbf{v} \cdot \nabla \mathbf{v} = \zeta \mathbf{k} \times \mathbf{v} + \frac{1}{2} \nabla \mathbf{v}$ is used to write the advection term in a vector invariant way, where $\zeta = \nabla \times \mathbf{v}$ is relative vorticity. The spatial discretization is a finite volume approximation for the divergence and curl operator. The gradient is approximated as a finite difference. The Leap-frog time integration scheme with Asselin filtering is used to prevent numerical instabilities from occuring. In the ICON and the Nambu discretization the spatial resolutions is approximately 85 km (10242 vorticity points, 30720 wind edges, 20480 height points) for this test.

2.3 The Nambu scheme

The Nambu scheme is a modification of the ICON spatial discretization scheme on the same grid. While being also a finite volume approximation in vector invariant form, it features a different averaging scheme and also the operator stencils are larger than those of the ICON scheme. Its construction method is based on the Nambu representation (Nambu 1973) of the shallow-water equations suggested in Salmon (2005) and Salmon (2007). This representation is a generalization of Hamiltonian representation, where the skew-symmetric Poisson bracket is replaced by a twofold skew-symmetric Nambu bracket. The associated spatially semi-discretized ODE conserves total energy and potential enstrophy algebraically exact. For the time integration, the leap-frog and the implicit midpoint method were analyzed. Time-step size was chosen 100 s which corresponds to a Courant number of 0.5. While none of the two methods conserves energy or potential enstrophy exactly, the implicit midpoint method reflects the conservation properties much better than the leap-frog scheme with Robert-Asselin filter. Hence we only show results with the implicit midpoint simulation. A semi-implicit implementation of the fully implicit midpoint rule can also be expected to outperform the leap-frog scheme with Robert-Asselin filter. The main difference between the ICON and the Nambu scheme lies in the use of different prognostic variables and different

averaging. The ICON scheme consists in a prognostic equation of the wind normal to triangle edges and height at triangle centers. The Nambu scheme on the contrary predicts vorticity at hexagon centers, and divergence and height at triangle centers. Wind velocity is then reconstructed from vorticity and divergence by solving the Poisson equations for the corresponding streamfunction and vector potential. The placement of the variables on the staggered grid is displayed in Fig. 2. To enable the conservation properties to be fulfilled, the averaging with the Nambu scheme takes places on a considerably larger stencil.

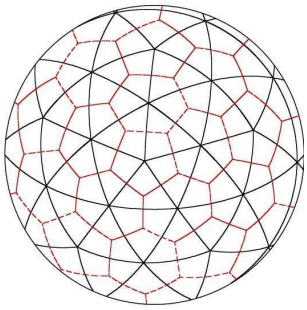

(a) The ICON grid at low resolution

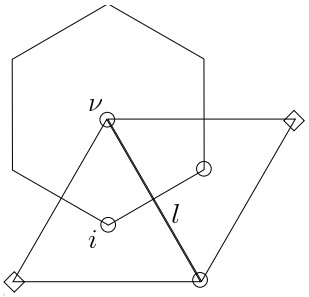

(b) The local stencil: Vorticity point ν, mass and divergence point i and wind edge l.

Figure 2: The ICON grid at low resolution and its local stencil.

PDE	Standard Discretization $\longrightarrow$	ODE / Conservative ODE
$\downarrow$		$\uparrow$
PDE in Nambu form	Nambu Discretization $\longrightarrow$	ODE in Nambu form

Table 1: Standard and Nambu discretization scheme

2.4 The HPM scheme

The HPM scheme in this study is a fully Lagrangian formulation which uses a set of K particles with coordinates $\mathbf{x}_k \in \mathbb{R}^3$ and velocities $\mathbf{v}_k \in \mathbb{R}^3$ (Frank & Reich 2004). The key aspects of the HPM lie in its variational or Hamiltonian nature of the spatial truncation and its combination with a symplectic time stepping so that it guarantees excellent conservation of mass, energy, and circulation. This distinctive feature is illustrated in Table 2 in comparison to standard methods. The HPM utilizes also a longitude-latitude grid with equal spacing π/J, over which a smoothing operator is implemented. Here J denotes the number of grid points in the latitudinal direction, and is 256 in this test so that the length of the grid is about 78 km longitudinally at the equator. The spatial discretization is combined with a modified RATTLE/SHAKE algorithm (Frank & Reich 2004). This explicit time-stepping is symplectic so that it ensures excellent conservation of total energy and circulation. The

time-step size used here is 28.8 minutes. A total of $K = 1335096$ particles are equidistributed over the sphere initially in this test.

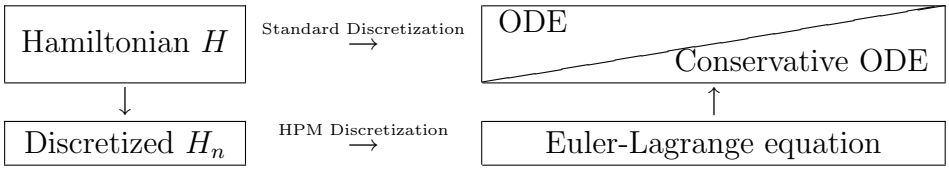

Table 2: Standard and HPM discretization scheme

3 Experiments and discussion

3.1 Vorticity fields

First, we initialize each model with the balanced zonal wind and integrate without the initial perturbation (Galewsky et al. 2004). This is to examine the ability of schemes in this study to maintain the steady zonal flow at least several days without diffusion. The zonal flow given in this test is dynamically unstable so that truncation errors can initiate instability even without the initial perturbation. For comparisons with the results in the reference (Fig. 4 in Galewsky et al. (2004)), we focus on the vorticity fields in the Northern Hemisphere (Fig. 3 and 4). The maintenance of the zonal jet is observed up to 7-8 days in the HPM simulation without the given perturbation. However, this test is not trivial for the schemes with the ICON grid which is not isotropic. Since the ICON grid is not zonally symmetric, the zonally symmetric initial state decays very quickly with the generation of non-zonal components. Wave 5 pattern develops dominantly and only little difference between the cases with or without the perturbation can be observed (Fig. 3 and Fig. 4). On the other hand, the wave structure at day 6 in the HPM simulation with the initial perturbation reasonably matches the reference solution. The inviscid evolution of the vorticity field is well captured when we examine the solution at time steps before day 6 (not shown here). The unstable vorticity field rolls up into a number of vortices and develops steep vorticity gradient as featured in Galewsky et al. (2004). The spatial resolution is refined for the ICON grid and it is observed that contour plots of vorticity fields change with further refinement and some features of the reference solution emerge. Moreover, wave 5 pattern weakens and its onset is delayed as the resolution increases. The effect of the ICON grid will be discussed more in the section 3.3.

3.2 Spectral analysis

In this section we use spectral analysis to examine how kinetic energy is transferred between wave numbers over time. In particular, we are interested in the long-term behaviour of the HPM and the Nambu discretization in this test. In accordance with turbulence theory for incompressible fluids we analyze the $\|\mathbf{v}\|^2$ fields. Let ε_{lm} be the spherical harmonic coefficient of the local constant height kinetic energy $\|\mathbf{v}\|^2$:

$$\varepsilon_{lm} = (\|\mathbf{v}\|^2, Y_{lm}) = \int \mathrm{d}\mathbf{A}\, \|\mathbf{v}\|^2 Y_{lm}, \tag{3.1}$$

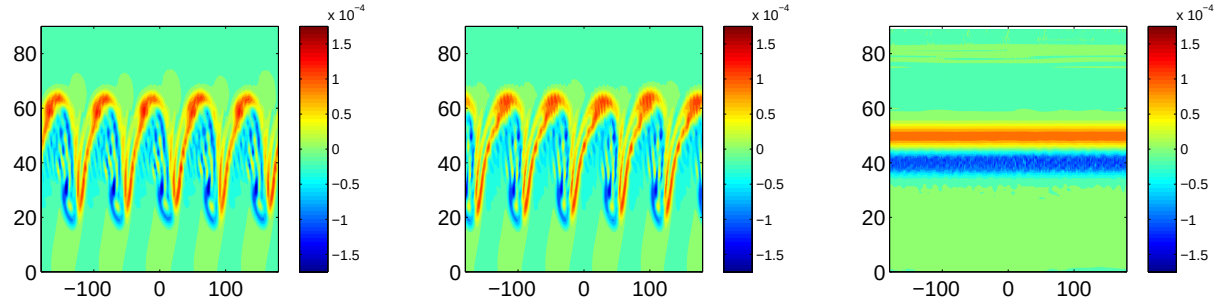

Figure 3: Vorticity fields without initial perturbation of ICOSWP (left), Nambu scheme (center) and HPM (right) at day 6

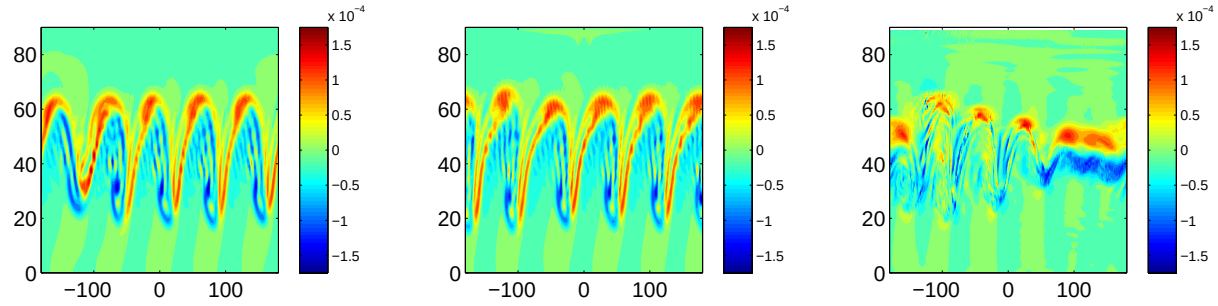

Figure 4: Vorticity fields with the given initial perturbation of ICOSWP (left), Nambu scheme (center) and HPM (right) at day 6

Here, Y_{lm} is the normalized spherical harmonic of degree l and order m. The integral in (3.1) is evaluated on the regular grid for HPM and on the ICON grid for the other two schemes. The spectral density of kinetic energy in degree l is then defined by

$$\varepsilon_l = \sum_{m=-l}^{l} |\varepsilon_{lm}|^2. \tag{3.2}$$

This spectral density of kinetic energy ε_l is shown in figure 5 for the test without the initial perturbation. It is shown that the peaks of spectrum are nearly unchanged in the HPM simulation (compare the right panel of Fig 1), consistent with its maintenance of zonal jet at this time (Fig. 3). Meanwhile, an increase in the kinetic energy on smaller scales is observed in the Nambu simulation, which is related to the development of the wave 5 pattern (the first two panels of Fig 3). However, it is observed that peaks of spectrum on larger scales have generally similar pattern to that at the initial time. The spectral density at day 25 (dash line) and 30 (dots) are also shown in Fig. 5. At 25 days, there is some increase of energy in the larger scales below wave number 10, as well as on smaller scales in simulations with the ICON grid. The spectrum of the HPM scheme is steeper than ICON and the Nambu schemes, which indicates more energy in larger scales and less in the smallest scales. The slight increase of small-scale energy is related to the development of complex flow associated with truncation error after day 6. The spectral density at day 25 and 30 days nearly overlap

each other in all schemes. This suggests that spectrum become stationary in the long-term simulation. It also demonstrates that these schemes are stable in the long-term integration.

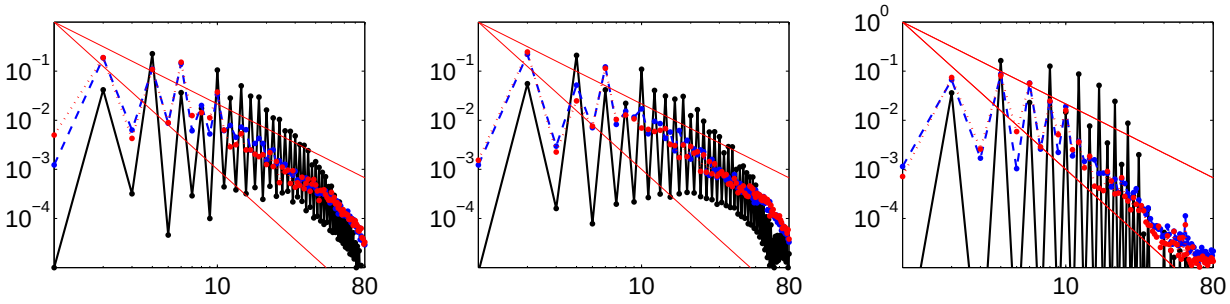

Figure 5: Spectral analysis for ICOSWP (left), Nambu scheme (middle), and HPM (right) at day 6 (black), 25 (blue), and 30 (red) from the test without the initial perturbation.

In the test with the initial perturbation, influences of the perturbation on the spectrum are well visible (Fig. 6): The odd modes become much more excited in the perturbed case than in the unperturbed case at day 6. The development of vortices in the HPM simulation corresponds to the increase of energy on larger wave numbers. The spectrum of the HPM scheme is generally steeper than that of the Nambu and the ICON schemes. Apparently the difference is largest in the smallest scales, which might be related to the differences in vortex structure. At day 25 and 30, increases of smallest-scale energy is evident in the ICON and the Nambu schemes, while energy transfer on that scale is minimal in the HPM scheme. As in the unperturbed test, the spectrum becomes stationary before 30 days and all schemes are stable in the long-term integration.

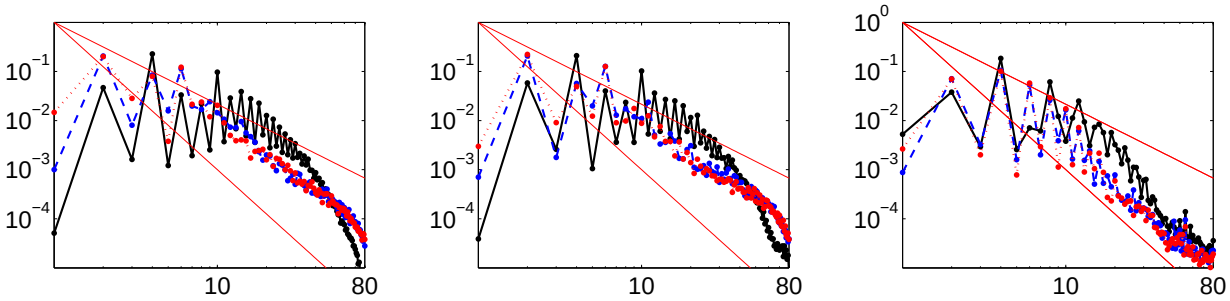

Figure 6: Spectral analysis for ICOSWP (left), Nambu scheme (middle), and HPM (right) at day 6 (black), 25 (blue), and 30 (red) from the test with the initial perturbation.

3.3 Effect of the ICON grid

In the previous sections it is shown that a wave 5 pattern develops in simulations with the ICON grid (both ICOSWP and Nambu scheme). This has raised a question whether an increase of spatial resolution delays or weakens the instability generation due to the non-isotropic grid. We examine this by simulating the test with doubled resolutions, i.e., 40 km

and 20 km. It is observed that the wave 5 pattern emerges later as the resolution increases (Fig. 7). Features (Rolling-up wave around the longitude -100°) in the reference solution are partially captured and the wave 5 pattern becomes less dominant. Spectral analysis using the 25 km simulation with the ICON scheme reasonably agrees to that using data from 80 km simulation (Fig. 8). Also this spectrum has better agreement with that in the HPM simulation in the long-term simulation (see spectral density at day 25 and 30).

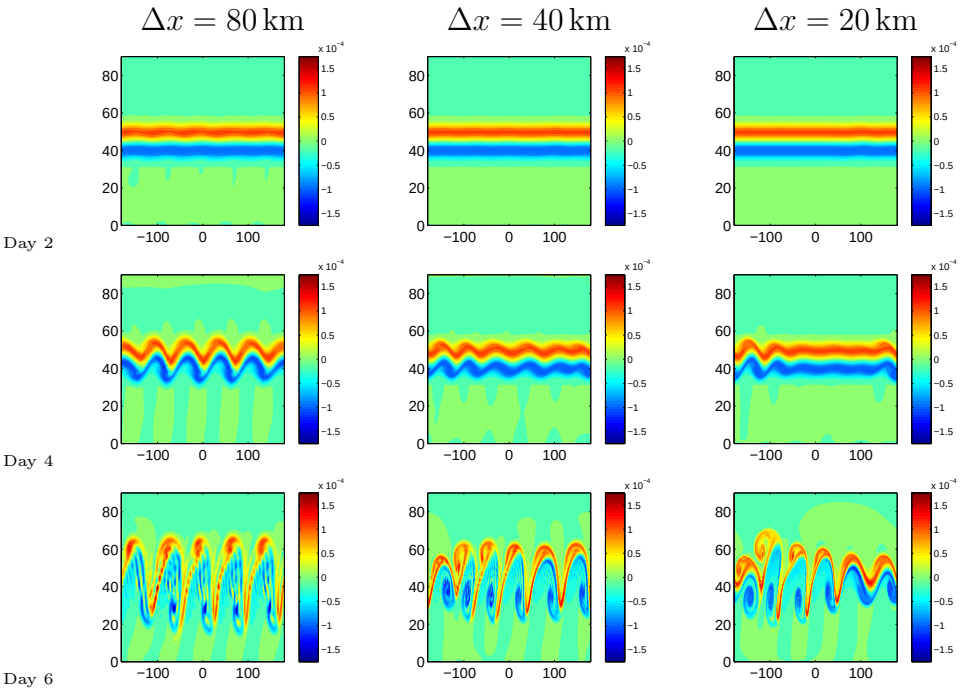

Figure 7: Vorticity fields with initial perturbation for ICOSWP.

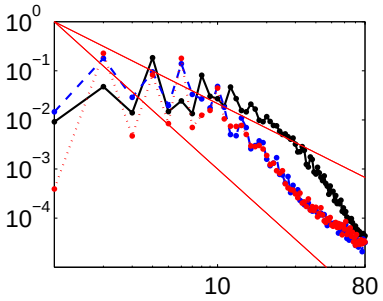

Figure 8: Spectral analysis for ICOSWP with the grid size of 25 km, at day 6 (black), 25 (blue), and 30 for the test with the initial perturbation.

3.4 Time series

Conservation of energy to a high degree of accuracy is observed in all simulations with ICOSWP, Nambu, and HPM scheme (Fig. 9). Meanwhile, the enstrophy is conserved best in the Nambu simulation. Here we define the potential enstrophy as $\mathcal{E} = 0.5 \sum_\mu h_\mu q_\mu^2 A_\mu$, where q is potential vorticity amid A_μ is the area of a grid cell of index μ. This definition might not yield enstrophy changes that represent the behaviour of the HPM scheme exactly due to approximations to obtain grid-based values from particle-based ones. Nevertheless, it is shown that the loss of enstrophy does not increase significantly with time. Together with spectral analysis this also suggests that the schemes used in this study remain stable in the long-term simulation.

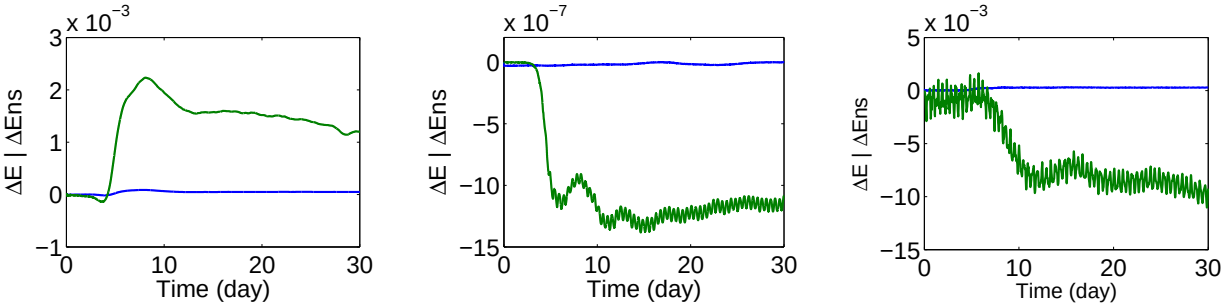

Figure 9: Time series of total energy (blue) and potential enstrophy (green) for ICOSWP (left), Nambu scheme (middle), and HPM scheme (right). Time series of potential enstrophy obtained using the approximated grid-based PV in the HPM simulation.

4 Conclusion and Outlook

The test used in this study has the advantage that it uses simple and analytic functions for initial conditions with a prescribed perturbation to impose barotropic instability. The HPM simulations could reproduce the vorticity fields similar to those in the reference test in (Galewsky et al. 2004). Without the perturbation the steady zonal jet is maintained up to 7-8 days without diffusion in the HPM simulations. However, the maintenance of a zonal jet with steep vorticity gradient is problematic to the schemes with the ICON grid since non-zonal components in association with the non-isotropic grid generate instability rapidly. This problem is solved partially by increasing the spatial resolution, but the wave pattern associated with the grid structure is persistent. It should be noted that relatively high computational cost for the Nambu discretization with the ICON grid is required to reproduce the solution close to the reference one. These results indicate that the grid chosen for constructing a conservative scheme affects the accuracy of solution significantly. As an outlook, this shortcoming could be addressed in future work in the ICON model. Meanwhile, all schemes in this study have some agreement in the evolution of spectral density in the long-term integration. This agreement increases especially with finer resolution in the ICON discretization, which is consistent with the improved accuracy in those simulations. All schemes remain stable for long-term integration, which is demonstrated by the

energy conservation to a high degree accuracy and spectral density distribution. The results in this test encourage further investigations with these conservative numerical schemes for describing atmospheric flows.

5 Acknowledgement

We thank two anonymous reviewers for their comments, which were helpful to improve the manuscript. This work was supported by the DFG project 'Structure preserving numerics'.

References

Bonaventura, L. & Ringler, T. 2005 , Analysis of discrete shallow-water models on geodesic Delaunay grids with C-Type staggering, Monthly Weather Review **133**, 2351–2371.

Frank, J. & Reich, S. 2004 , The hamiltonian particle-mesh method for the spherical shallow water equations, Atmospheric Science Letters **5**, 89–95.

Frank, J., Gottwald, G. & Reich, S. 2002 , The Hamiltonian particle-mesh method, in M. Griebel & M. Schweitzer, eds, 'Meshfree Methods for Partial Differential Equations', Vol. 26 of **Lecture Notes in Computational Science and Engineering**, Springer-Verlag, Berlin Heidelberg, pp. 131–142.

Galewsky, J., Scott, R. & Polvani, L. 2004 , An initial-value problem for testing numerical models of the global shallow-water equations, Tellus A **56**, 429–440.

Nambu, Y. 1973 , Generalized hamiltonian dynamics, Phys. Rev. D **7**(8), 2405–2412.

Névir, P. & Blender, R. 1993 , A nambu representation of incompressible hydrodynamics using helicity and enstrophy, Journal of Phyics. A **26**, 1189–1193.

Salmon, R. 2005 , A general method for conserving quantities related to potential vorticity in numerical models, Nonlinearity **18**(5), R1–R16.

Salmon, R. 2007 , A general method for conserving energy and potential enstrophy in shallow-water models, Journal of Atmospheric Science **64**, 515–531.

Shin, S. & Reich, S. 2009 , Hamiltonian particle-mesh simulation for a non-hydrostatic vertical slice model, Atmospheric. Science. Letters. In press.

Sommer, M. & Névir, P. 2009 , A conservative scheme for the shallow-water system on a staggered geodesic grid based on a nambu representation, Quarterly Journal of Royal Meteorological Society **135**, 485–494.